PERFORMANCE OF A NOVEL HELIUM-STIRRED SOLID OXIDE FUEL CELL WITH MOLTEN METAL ANODE FOR ELECTRICITY GENERATION AND OXYGEN DISSOLUTION IN MOLTEN METAL

Agbede O. O.[*, 1], Hellgardt K.[2] and Kelsall G.H. [2]

1. Department of Chemical Engineering, Ladoke Akintola University of Technology Ogbomoso, P.M.B. 4000, Ogbomoso, Nigeria

2. Department of Chemical Engineering, Imperial College London, London SW7 2AZ, UK

[*]Corresponding author, email: ooagbede@lautech.edu.ng

ABSTRACT

A novel helium-stirred solid oxide fuel cell (SOFC) with a molten metal anode for electricity generation and oxygen dissolution in a molten metal was investigated. This SOFC configuration employs conventional cathode and electrolyte but incorporates a molten metal contained in an alumina crucible as anode and inert gas stirring of the molten metal. Tin was the metal used in this study because it is non-toxic and inexpensive, it also has a relatively low melting point and very low vapour pressure at high temperatures. The performance of a SOFC with molten tin anode at 850 ^oC was evaluated by the techniques of electrochemical impedance spectroscopy, cyclic voltammetry and chronoamperometry. A peak power density of ca. 100 W m^{-2} at a potential difference of ca. 0.45 V and current density of ca. 222 A m^{-2} was achieved. Impedance spectra showed that ohmic potential losses controlled the reactor performance, with about 59% of those arising from the inherent difficulty in achieving a low resistance contact at the silver wire (silver wool) current collector | cathode interface. The molten metal bath provided a relatively large reservoir of molten metal for oxygen absorption and transport compared to a thin film of molten metal while gas stirring of molten metal enhanced the transport of dissolved oxygen atoms from the yttria stabilized zirconia (YSZ) electrolyte | molten metal interface to the bulk molten metal and assisted in preventing oxide formation at the YSZ electrolyte | molten metal interface.

Keywords: solid oxide fuel cell, molten metal anode, YSZ electrolyte, electricity, tin, oxygen

1. Introduction

The Solid Oxide Fuel Cell (SOFC) is an electrochemical energy conversion device which converts the chemical energy in fuels directly to electrical energy; it consists basically of a porous oxygen reducing cathode, a dense oxide ion conducting solid oxide electrolyte and a porous fuel oxidizing anode (Ormerod, 2003). SOFCs have high efficiencies, no moving parts, quiet operation and low emissions at the point of use compared to conventional power plants (Brett et al., 2008). Hydrogen is the conventional fuel that is oxidized in a fuel cell, however, due to its high operating temperature (500 – 1000 ^oC), the SOFC can in principle be powered with carbonaceous fuels including natural gas, liquid hydrocarbons, coal and biomass (Ormerod, 2003; Minh, 2004). The conventional SOFC anode is a cermet of nickel and yttria stabilized zirconia (Ni-YSZ). Although carbonaceous fuels may be oxidized at the Ni-YSZ anode of the SOFC, there are still limitation to the cell performance when this anode is used; these include carbon formation which blocks anode surface e.g. due to methane cracking, poor contact of anode with solid fuels, anode poisoning due to sulphur present in fuel reacting with nickel, sintering of nickel in the Ni-YSZ anode and instability due to redox cycling of nickel anode which could lead to mechanical failure of the cell (Matsuzaki & Yasuda, 2000; Gorte et al., 2002; Kurokawa et al., 2007; Sarantaridis et al., 2008; Nikolla et al., 2009; Offer et al., 2009).

Recent research interest is in the use of molten metal anodes in place of the conventional Ni-YSZ anode in SOFCs for the direct oxidation of gaseous, liquid and solid carbonaceous fuels; these anodes are able to obviate the challenges encountered in the direct oxidation of carbonaceous fuels in SOFCs. They have relatively higher tolerance for sulphur compared to the Ni-YSZ anode and unlike Ni-YSZ, they do not catalyse carbon formation. Besides, improved charge transfer is achievable when the SOFC is fuelled with solid carbon fuels (Tao, 2005; Tao et al., 2007; Tao et al., 2008). They are also good electronic conductors and current collection from such anodes is easier. Metals being explored as molten anodes usually have low melting points and low vapour pressures at high temperatures, they include antimony (Jayakumar et al., 2010a; Jayakumar et al., 2010b; Jayakumar et al., 2011; Javadekar et al., 2012a; Wang et al., 2013; Cao et al., 2014; Wang et al., 2014a; Wang et al., 2014b), bismuth (Jayakumar et al., 2010a; Jayakumar et al., 2010b), copper (Jacob, 2011), indium (Jayakumar et

al., 2010a; Jayakumar et al., 2010b), tin (Tao et al., 2007; Gemmen et al., 2010; Jayakumar et al., 2010a; Jayakumar et al., 2010b; McPhee et al., 2011; LaBarbera et al., 2012; Wang et al., 2014c; Khurana et al., 2015), silver (Javadekar et al., 2012b), lead (Jayakumar et al., 2010a; Jayakumar et al., 2010b) and some alloys (LaBarbera et al., 2011). The SOFCs with molten metal anodes reported in the literature comprised of designs which used a thin layer of metal as anode. Such cell designs were plagued by rapid oxide formation at the molten metal anode | electrolyte interface due to slow diffusion of oxygen atoms in such quiescent systems and sluggish fuel reaction with oxygen atoms (Jayakumar et al., 2010a; Jayakumar et al., 2010b; Wang et al., 2014c). The metal oxide covered the electrolyte and consequently limited charge transfer and cell performance. One solution to this problem is to increase the diffusion of oxygen atoms away from the molten metal anode | electrolyte interface to avoid accumulation of oxygen atoms and subsequent formation of oxide at this interface. Likewise, the slow diffusion of gaseous fuel species (e.g. hydrocarbons) heavier than hydrogen, is a challenge to be overcome in systems where porous ceramic separators were used to separate molten metal from fuel such that there was no direct contact between fuel and molten metal (Tao et al., 2008). In some other designs in which the surface of the molten metal was simply exposed to gaseous fuels, oxygen–fuel reaction was limited to the exposed surface of the molten metal since the gaseous fuel (e.g. hydrogen) solubility in molten metal (e.g. tin) is extremely small (Abernathy et al., 2011; LaBarbera et al., 2012; Khurana et al., 2015).

The injection of gas bubbles into molten metal is expected to enhance diffusion within the molten metal and the reaction of gaseous fuel with oxygen atoms. A novel SOFC with molten metal anode which incorporates a molten metal bath and gas bubbling is being investigated; this cell is expected to obviate the challenges encountered in the direct oxidation of carbonaceous fuels in SOFCs. In addition, a large molten metal bath coupled with gas bubbling would provide a larger capacity for oxygen absorption (and energy storage), enhance oxygen diffusion and prevent oxide formation at the molten metal | electrolyte interface. Hence, the objectives of this study were to demonstrate and characterize a novel SOFC with molten metal anode ($M_{(l)}$-SOFC) which is stirred with an inert helium gas while being operated in battery mode or as an electrochemical device for oxygen dissolution in a molten metal.

2. The Novel SOFC with Molten Metal Anode

Figure 1 shows the schematic of the novel $M_{(l)}$-SOFC investigated, it consists of conventional cathode (Lanthanum strontium manganite - $La_{0.8}Sr_{0.2}MnO_3$ - LSM) and electrolyte (yttria doped zirconia - ZrO_2-Y_2O_3 -YSZ) but a molten metal anode. This cell incorporates a molten metal bath and gas bubbling. This design is expected to provide enhancement for oxygen diffusion in the molten metal anode, a higher capacity for oxygen absorption (and energy storage) and larger surface area for gaseous fuel-oxygen atom reaction compared to previously reported $M_{(l)}$-SOFCs which utilized a thin layer of molten metal or simply exposed the surface of the molten metal to gaseous fuels. Oxide formation may be avoided on the surface of the YSZ electrolyte since molten metal agitation by gas bubbles enhances the diffusion of oxygen atoms away from the molten metal | YSZ electrolyte interface while the large quantity of molten metal in the reactor implies a relatively larger conduit for oxygen absorption and transport to bubble | molten metal interfaces compared to a thin film of molten metal.

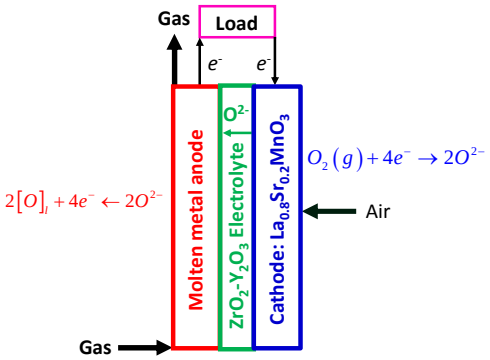

Figure 1: Schematic of a SOFC with molten metal anode

Oxygen reduction occurs at the cathode and oxide ions (O^{2-}) are conducted through the electrolyte to the electrolyte | molten metal interface where they are oxidized to oxygen atoms which dissolve in the molten metal ($[O]_l$). The electrons released pass through an external load to the cathode while the oxygen atoms diffuse to the bulk molten metal and bubble | molten metal interfaces where they may react with e.g. a gaseous fuel if present at the anode. The reactions in this $M_{(l)}$-SOFC are:

Cathode (LSM): $$O_2(g) + 4e^- \rightarrow 2O^{2-} \quad [1]$$

Electrolyte (YSZ): $$2O^{2-}(cathode) \rightarrow 2O^{2-}(anode) \quad [2]$$

YSZ | Molten metal anode interface: $$4e^- + 2[O]_l \leftarrow 2O^{2-} \quad [3]$$

If a gaseous fuel e.g. methane is present, then it may react with dissolved oxygen atoms:

Methane bubble | Molten metal interface: $4[O]_l + CH_4(g) \rightarrow 2H_2O(g) + CO_2(g)$ [4a]

or $[O]_l + CH_4(g) \rightarrow CO(g) + 2H_2(g)$ [4b]

It is also possible for the oxide ion to react with molten metal (M) at the YSZ | molten metal interface to form the metal oxide (e.g. MO_2) depending on current densities and local mass transport rate coefficients:

YSZ | Molten metal interface: $MO_2(s) + 4e^- \leftarrow 2O^{2-} + M(l)$ [5]

However, in this study, the use of a molten metal bath coupled with gas stirring of the molten metal is expected to prevent solid oxide formation at the YSZ | molten metal interface which would have prevented further charge transport and limit cell performance (Tao et al., 2007; Jayakumar et al., 2010b).

When no fuel is fed to the anode while current is drawn from the cell, only reactions [1], [2] and [3] occur and oxygen is just pumped into or dissolved in the molten metal anode, the cell is said to be operated in battery mode or as a device for dissolving oxygen in the molten metal. Also, for a fuelled $M_{(l)}$-SOFC, when the cell is operated at high current densities above a particular threshold, the rate of dissolution of oxygen atoms in the molten metal would exceed the rate of fuel reaction with oxygen atoms which would result in the accumulation of dissolved oxygen atoms in the molten metal; in such situation, the cell is also said to be operated in battery mode (Tao et al., 2007).

The $M_{(l)}$-SOFCs, as an electrochemical device for oxygen dissolution in a molten metal, may be utilised for a continuous dissolution of oxygen in a molten metal with simultaneous (at the cell anode) or subsequent (in a separate reactor) contacting of dissolved oxygen atoms with e.g. methane at the molten metal interface for methane conversion to synthesis gas (hydrogen and carbon monoxide) or oxygenates. This technique of electrochemically dissolving oxygen in a molten metal, while still generating electricity from the cell, may also be employed in metal refining instead of directly using oxygen gas. The helium-stirred $M_{(l)}$-SOFC was investigated (in battery mode and) as a device for oxygen dissolution in molten metal to evaluate the efficacy of a large molten metal bath and gas stirring in preventing oxide formation at the electrolyte | anode interface especially when the cell is operated at high current densities.

Tin was the metal used in this investigation because it is non-toxic and inexpensive, it also has a relatively low melting point (232 ^oC) and very low vapour pressure at high temperatures (boiling point is 2603 ^oC).

3. Experimental

3.1. Materials

The electrolyte was a one-end closed 10.5% yttria doped zirconia (10.5% YSZ) tube obtained from McDanel Advanced Ceramic Technologies, LLC, Pennsylvania, USA; it had an outer diameter of 6.35 mm, an inner diameter of 4.78 mm and a length of 327 mm. Lanthanum strontium manganite ($La_{0.80}Sr_{0.20}MnO_3$ - LSM) paste and LSM-YSZ (50 wt% $La_{0.80}Sr_{0.20}Mn0_3$ and 50 wt% $(Y_2O_3)_{0.08}(ZrO_2)_{0.92}$,) paste, as well as the vehicle ink for diluting the pastes, were purchased from NexTech Materials (Fuelcellmaterials.com) Ohio, USA. Tin granules were obtained from Sigma Aldrich, these had a maximum impurity of 0.05% antimony, 0.02% bismuth, 0.01% copper, 0.02% iron, and 0.05% lead. Silver wire (0.25 mm diameter and 999.9 % pure) was obtained from Sigma Aldrich while graphite rod (3.05 mm diameter, 305 mm long, and 99.9995 % pure) and silver wool (99.9+ % pure) were purchased from Alfa Aesar. Helium (grade A purity) was acquired from BOC Ltd, UK while air was generated in the laboratory from a Chrompack AO100 air generator.

3.2. Laboratory Electrochemical Reactor Design and Experimental Apparatus

A SOFC with molten tin anode ($Sn_{(l)}$-SOFC) was investigated; the laboratory electrochemical reactor basically consisted of YSZ electrolyte, double-layered LSM-YSZ/LSM cathode and molten tin anode. The double-layered cathode was fabricated on the inside of the one-end closed YSZ tube; the inside of the YSZ tube was first coated with LSM-YSZ paste, dried and sintered in air at 1100 ^oC for 3 hours using a Carbolite STF 15/76 furnace, it was then coated again with the LSM paste, dried and sintered a second time to obtain a double-layered LSM-YSZ/LSM cathode. Silver wire and graphite rod were used as the current collectors for the cathode and anode, respectively. Silver wool was also inserted inside the electrolyte to enhance the contact between the silver wire current collector and the cathode. The experimental apparatus used in this study is shown in Figure 2. Molten tin was contained in an alumina crucible (placed in a furnace) which had a height of 300 mm, an inner diameter of 70 mm and a thickness of 5 mm; the depth of molten tin in the alumina crucible was ca. 115 mm. The YSZ electrolyte tube (which had an LSM-YSZ/LSM double-layered cathode fabricated on its inside), graphite current collector and an alumina gas feed tubing (nozzle) were inserted into the alumina

crucible through fittings on its lid which had been secured with flanges. The base (closed end) of the YSZ tube, graphite rod and tip of the alumina gas feed tubing were immersed ca. 65, 20 and 100 mm, respectively, below the molten tin surface. The helium flowrate was set by an electronic mass flow controller supplied by Bronkhorst (UK) Ltd, while air was fed to the cathode from a Chrompack air generator at a flow rate of 30 ml min^{-1}. The molten tin anode temperature was calibrated with the furnace temperature setting by a stainless steel sheath K type thermocouple purchased from RS component, to ensure that the thermocouple was not left in the reactor for a long time thereby preventing its dissolution in the molten tin. Electrochemical measurements were performed using an AUTOLAB PGSTAT30 potentiostat equipped with a frequency response analyser and Nova software (Eco Chemie, Netherlands); the cathode current collector was connected to the counter and reference electrodes of the potentiostat while the anode current collector was connected to the working and sense electrodes.

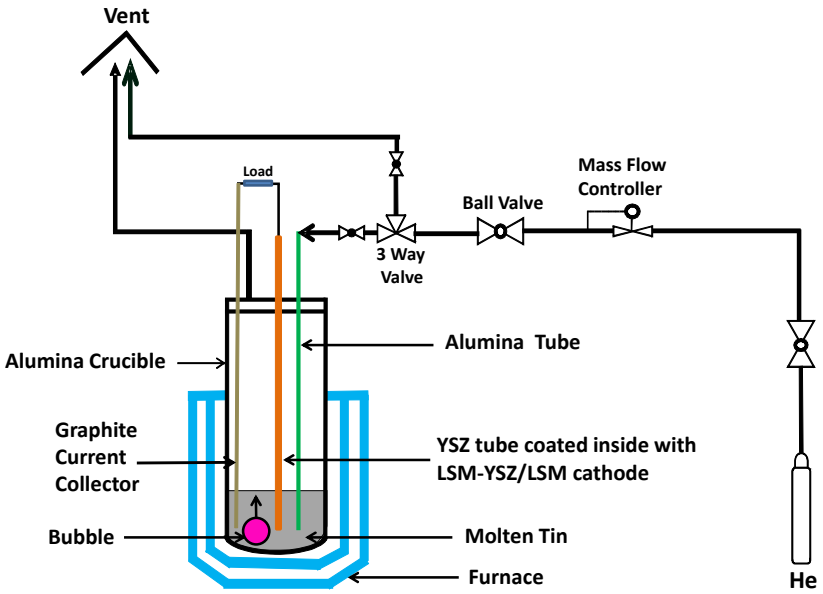

Figure 2: Schematic of experimental arrangement

3.3. Experimental Procedure

The experimental apparatus shown in Figure 2 was utilized to determine the actual performance of the fuel cell when the molten tin anode was stirred with helium. The reactor was sealed up and helium, at a flow rate of 60 ml min^{-1}, was bubbled through the molten tin as it was heated to the operating temperature of 850 ^{o}C. Air was fed to the cathode at a flow rate of 30 ml min^{-1}. The measured open circuit potential difference of the cell was recorded and monitored continuously until it became stable. The techniques of electrochemical impedance spectroscopy (EIS), cyclic voltammetry (CV) and chronoamperometry were then applied to the $Sn_{(l)}$-SOFC operated at 850 ^{o}C, for further characterization. A frequency range of 10 kHz – 10 mHz and amplitude of 0.01 V were employed at open circuit potential difference for the EIS studies; impedance-frequency relationships were displayed in Nyquist plots. In the CV study, the cell potential was ramped using a ramp rate of 100 mV s^{-1} from the open circuit voltage to zero and back to the open circuit voltage; 2 to 4 cycles were used. Potential difference – current density and power density-current density curves, which possess features characteristic of the reaction mechanism and kinetic conditions of the electrochemical cell, were then drawn from the data obtained. The technique of chronoamperometry was used to investigate the stability of the fuel cell performance when a constant potential was applied to it for a period of time. The cell potential was stepped from the open circuit value to the value at peak current density while measuring the current as a function of time; this provided information about the cell processes that occurred at the molten tin anode at a set potential which corresponded to the peak current density. The total surface area of 1.3×10^{-3} m^2 of the anode in contact with the electrolyte was used in computing the area specific resistances (impedances), current and power densities.

4. Results and Discussion

4.1. $Sn_{(l)}$-SOFC Performance

The cell investigated was:

$$He, Sn(l) \mid 10\%Y_2O_3 - ZrO_2 \mid LSM - YSZ, LSM, air \quad (1)$$

The open circuit potential difference was determined to be stable at ca. 0.89 V, which is higher than the Nernst potential for the saturation of molten tin with dissolved oxygen and the oxidation of molten tin to SnO and SnO_2 at 850 °C. The bubbling of helium through molten tin caused the degassing of dissolved oxygen atoms from the molten tin (Papamantellos et al., 1971; Dantzig et al., 1980; Sano & Mori, 1982; Huang et al., 2002; Warke et al., 2005). At open circuit, the helium gas kept the oxygen at the anode from being in equilibrium with tin oxides by lowering the chemical potential of oxygen in the molten tin below the requirement for oxide formation.

Figure 3a shows the potential difference-current density (U-j) polarization curve for the helium-stirred SOFC with molten tin anode for two cycles of potential difference sweeps from the open circuit potential difference to zero and back to the open circuit potential difference at a ramping rate of 10 mV s^{-1}.

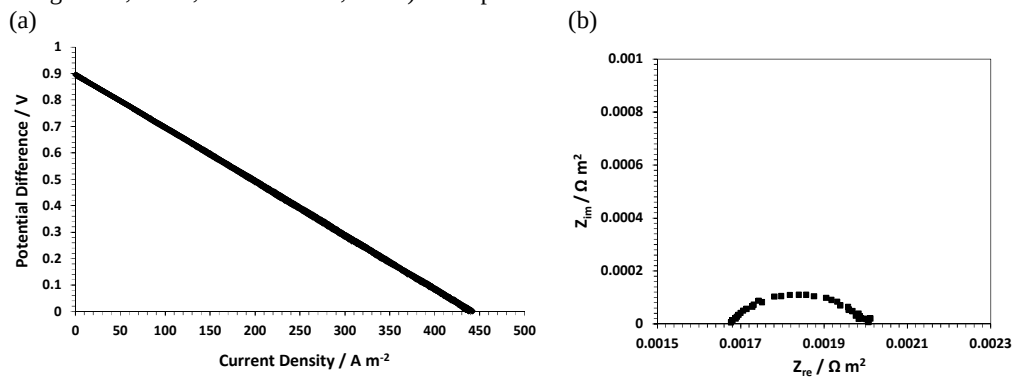

Figure 3: (a) U-j data for helium stirred SOFC with molten tin anode at 850 °C (first set of measurements - 2 cycles) (b) Impedance spectrum of helium stirred SOFC with molten tin anode at open circuit, 850 °C and frequency range of 100 mHz - 10 kHz (measurement taken prior to any U-j cycling)

The polarization curve shows that the open circuit potential difference decreased with increasing current density from the open circuit value to zero and was restored back to its initial value after two cycles of potential sweeps. The *U-j* behaviour was reversible and linear, which implies that the potential losses were due mainly to ohmic potential losses in the electrolyte and contacts. The impedance spectrum shown in Figure 3b, which was obtained at open circuit and frequency range of 100 mHz - 10 kHz, also confirmed this. The ohmic impedance obtained from the high frequency intercept with the real axis was 1.7×10^{-3} Ω m^2, while the non-ohmic impedance determined from the difference between the low and high frequency intercepts with the real axis was 3.02×10^{-4} Ω m^2. This ohmic impedance was ca. 85 % of the total impedance, which implies that ohmic potential losses controlled the reactor performance. The estimated resistance of the YSZ electrolyte was 2.26×10^{-4} Ω m^2. An analysis of this ohmic resistance showed that ca. 59 % of it was contact resistance, which was enormous, largely due to the inherent difficulty in achieving a low resistance contact at the silver wire (silver wool) current collector | cathode interface. The total surface area of 1.3×10^{-3} m^2 of the anode in contact with the electrolyte was used in computing the area specific resistances (impedances), current and power densities. The impedance spectra obtained before and after the polarization curve of Figure 3a are shown in Figure 4a; there was no increase in both the ohmic and non-ohmic impedance after the two cycles of potential sweep from the open circuit potential difference to zero and back to the open circuit potential.

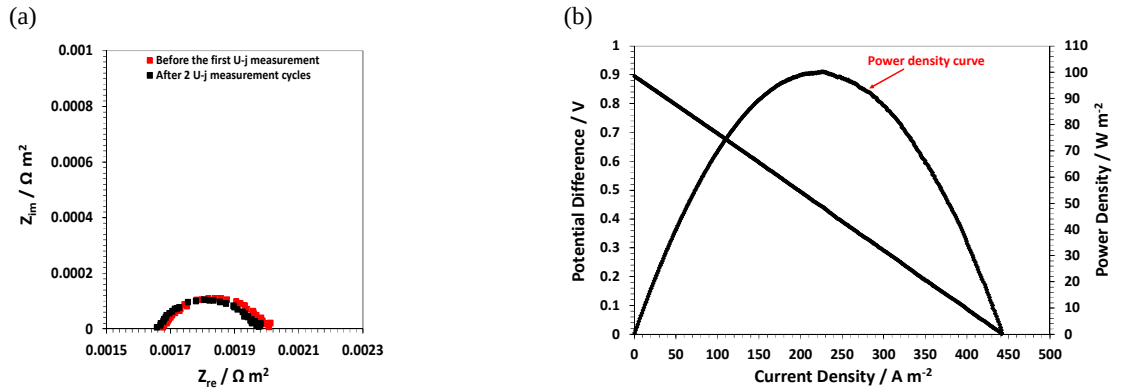

Figure 4: (a) Impedance spectrum of helium stirred SOFC with molten tin anode at open circuit, 850 °C, and frequency range of 100 mHz - 10 kHz (b) U-j and power density data of helium stirred SOFC with molten tin anode at 850 °C

Jayakumar et al. (2010b) studied the electrochemical oxidation of molten tin as anode for SOFC; they used a pellet (wafer) cell design, YSZ electrolyte, $La_{0.8}Sr_{0.2}FeO_3$-YSZ (LSF-YSZ) composite cathode and the thickness of their molten tin anode layer was 1.5 mm. They reduced the molten tin with hydrogen before the potential sweep experiment. The polarization curve they obtained after the potential difference was ramped at 10 mV s^{-1} from open circuit to zero and back, and the impedance spectra obtained before and after the potential sweep showed a decrease in the current density, an increase in the impedance and degradation of the cell after the charge transfer. They proved that these observations were due to the formation of solid tin dioxide at the YSZ | molten tin interface which hindered further charge transfer. The degradation of cell performance due to tin oxide formation at the YSZ | molten tin anode interface has also been reported by other investigators (LaBarbera et al., 2011; LaBarbera et al., 2012).

The *U-j* polarization curve and the impedance spectra of Figure 3a and Figure 4a, respectively, reveal that no cell degradation was observed in this study after two cycles of potential sweep unlike the system reported by Jayakumar et al. (2010b) in which degradation of the cell occurred due to SnO_2 formation at the YSZ | molten tin interface after a single cycle of potential sweep. This was partly due to the large volume of molten tin in the reactor compared to the magnitude of charge transferred and also because the continuous stirring of molten tin by the helium gas enhanced diffusion of dissolved oxygen atoms and consequently prevented the accumulation of dissolved oxygen atoms at the YSZ | molten tin anode interface and formation of tin oxide. Physical examination of the YSZ tube surface after the experiment confirmed that no SnO_2 was deposited on its surface. Hence, the reactor design used in this study which incorporates a large molten tin bath coupled with gas bubbling has a greater capacity for oxygen absorption and prevention of oxide formation at the YSZ | molten tin interface compared to the cell design of Jayakumar et al. (2010b) which used a thin film (1.5 mm thick) of molten tin, and those of other researchers (LaBarbera et al., 2011; LaBarbera et al., 2012) who used a molten metal bath but without gas bubbling. The U-j polarization and power density curves for the helium stirred cell obtained at 850 °C are shown in Figure 4b; a peak power density of ca. 100 W m^{-2} at a potential difference of ca. 0.45 V, and current density of ca. 222 A m^{-2} was achieved. The current density and consequently the power density obtained in this study have been largely limited by ohmic losses especially the inherent contact resistance in this cell arrangement, as previously discussed.

4.2. Effect of Cathode Contact Resistance

The *U-j* polarization and power density curves for the first and 24th cycle of potential sweep are shown in Figure 5a. The current density and consequently the power density had increased after the 24th cycle of *U-j* cycling, which was measured after about 7.5 hours of cell operation at 850 °C. A possible explanation of this increase in current density is that it was the result of the sintering or densification of the silver wool (used at the cathode for current collection) at 850 °C, the temperature at which the experiment was performed. The densification or compaction of the silver wool would have decreased the contact resistance at the silver wool | cathode interface, resulting in better current collection. Figure 5b shows a comparison of the impedance spectra before the first *U-j* measurement and after the 24th measurement; the ohmic impedance had decreased from 1.677 mΩ m^2 observed before the first U-j measurement to 1.587 mΩ m^2 after the 24th *U-j* measurement while the non-ohmic impedance had remained essentially constant. This confirmed that the observed change in the current density was due to a decrease in the cell's ohmic resistance. Visual observation of the silver wool when it was

taken out of the YSZ tube after the experiment further confirmed that it had been compacted during the cell operation at 850 °C (melting point of silver is 961.8 °C).

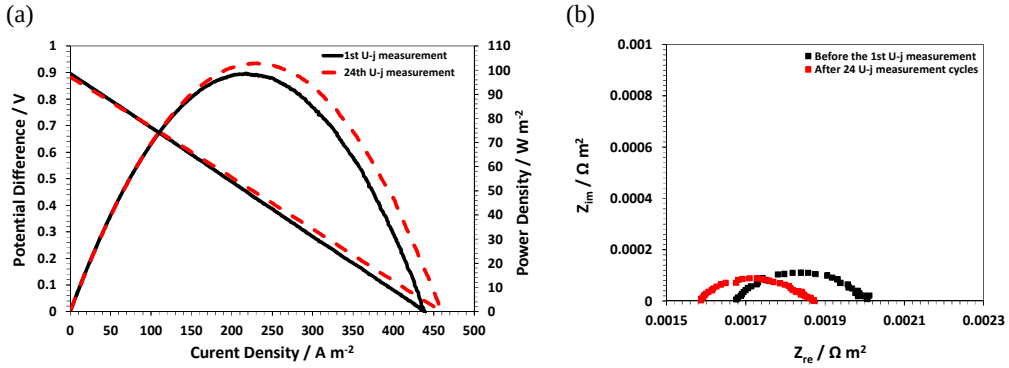

Figure 5: (a) U-j polarization and power density curves of helium stirred SOFC with molten tin anode at 850 °C for the 1st and 24th U-j measurement (b) Impedance spectra of helium stirred SOFC with molten tin anode before the 1st and after the 24th U-j measurement cycles at open circuit, 850 °C and frequency range of 100 mHz - 10 kHz

Contact resistance have been known to significantly lower the performance of SOFCs; Jiang (2001) used special voltage probes to measure separately the contact resistance at the current collector | cathode and current collector | anode interfaces and showed that the contact resistances at these interfaces can contribute considerably to the total cell resistance. Foger et al., (1999) also achieved ca. 70% reduction in total cell resistance from 1.09 to 0.3 Ω cm^2 at 750 °C by improving the contact between the electrode with additional contact layer and silver mesh. It has also been shown that the contact area of the current collector significantly affect the cell performance; Jiang et al. (2003) studied the effect of contact between electrode and current collector on the performance of solid oxide fuel cells using current collector with various contact area. They showed that the cell resistance and polarization losses of the cell decreased significantly when the contact area between the current collector and the cathode was increased; when the contact area of the current collector was increased from 4.6% to 27.2%, there was a corresponding decrease in cell resistance by ca. 80% from 1.43 to 0.19 Ω cm^{-2} at 800 °C. Discrete and inhomogeneous contacts between electrode and current collector cause uneven current distribution in porous electrodes especially in porous electrodes with low electrical conductivity, which lead to higher cell resistances and polarization losses (Sasaki et al., 1996; Jiang et al., 2003). Hence, there is the need to lower the contact resistance at the silver wire (silver wool) | cathode interface in the SOFC design investigated, in order to improve the cell performance. Colet Lagrille & Kelsall (2013) have also recently predicted, using the kinetic parameters for a planar cell configuration of a quiescent molten tin anode SOFC with a 2 mm thick electrolyte and assuming negligible ohmic losses due to current collection and contact resistances, that a peak power density of ca. 427 W m^{-2} at a current density of ca. 1 046 A m^{-2} and potential difference of ca. 0.41 V could be achieved at 900 °C in the absence of a fuel at the anode. This also shows that the performance of the reactor configuration investigated in this study could be improved by the elimination of the enormous contact resistance.

4.3. Oxygen Accumulation in Molten Tin

The stability of the cell was investigated by operating the cell at a constant potential of 0.45 V, corresponding to the peak power density, while the equivalent time dependence of the current density was monitored. The time dependence of the current and power densities are presented in Figure 6a; the increase in current and power densities was possibly due to decreasing contact resistance, as discussed earlier.

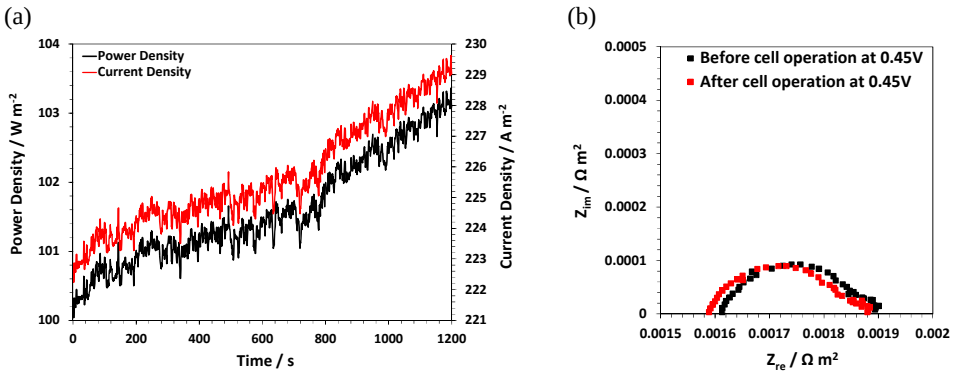

Figure 6: (a) Time dependence of power density of the helium stirred SOFC with molten tin anode at 0.45 V and 850 °C (b) Impedance spectra of helium stirred SOFC with molten tin anode before and after cell operation at 0.45 V, open circuit, 850 °C and frequency range of 100 mHz -10 kHz.

Oxygen was pumped into the molten tin while the cell was operated at this potential difference for 20 minutes; the impedance spectra presented in Figure 6b did not show any significant change in either the ohmic or non-ohmic impedances after the oxygen pump-in experiment.

Figure 7a shows the time dependence of the potential difference and current density when a 0.01 Ω resistor was connected across the cell. This load corresponds to the potential difference being stepped from the open circuit to ca. 0.14 V; the load was applied for 30 minutes and oxygen was pumped into the molten tin at this potential. The power density increased initially, probably due to the decrease in contact resistance earlier discussed, fluctuated about a mean power density of 52 W m^{-2}, before decreasing as the oxygen pump-in (dissolution) process progressed. The impedance spectra obtained before and after the potential difference was stepped to 0.14 V are shown in Figure 7b; there was no significant change in the impedance after stepping the potential difference from the open circuit to 0.14 V for 30 minutes. The ohmic impedance would have increased if tin oxide had been formed at the YSZ electrolyte | molten tin interface.

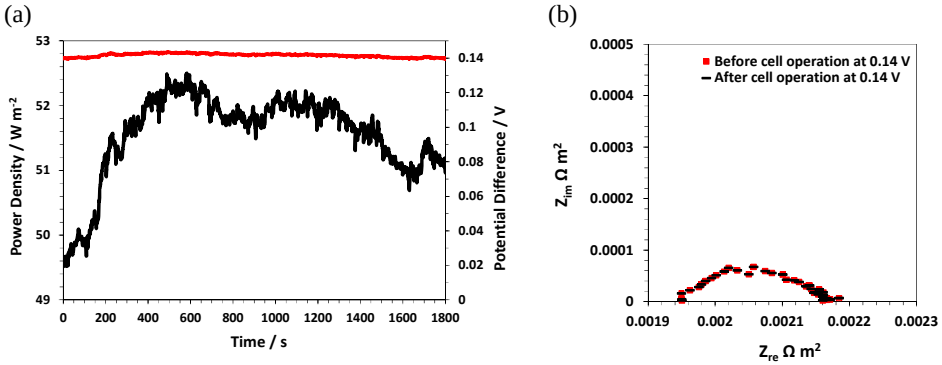

Figure 7: (a) Time dependence of potential difference and power density of helium stirred SOFC with molten tin anode with a load of 0.01 Ω at 850 °C (b) Impedance spectra of helium stirred SOFC with molten tin anode before and after cell operation at ca. 0.14 V, measured at open circuit, 850 °C and frequency range of 10 mHz - 10 kHz

The time dependence of power density obtained when the potential difference was stepped from the open circuit to 0.1 V for 45 minutes is presented in Figure 8a. The power density increased initially, then decreased as the oxygen pump-in process progressed; the observed decrease in the power density was due to the resultant accumulation of dissolved oxygen atoms in the molten tin. The *U-j* polarization and power density curves before and after the potential difference was stepped from the open circuit to 0.1 V are shown in Figure 8b; the open circuit potential difference, highest current density, and peak power density decreased from ca. 0.89 V to ca. 0.865 V, ca. 445 A m^{-2} to ca. 165 A m^{-2} and ca. 96 W m^{-2} to ca. 38 W m^{-2}, respectively, due to the accumulation of dissolved oxygen atoms in the molten tin.

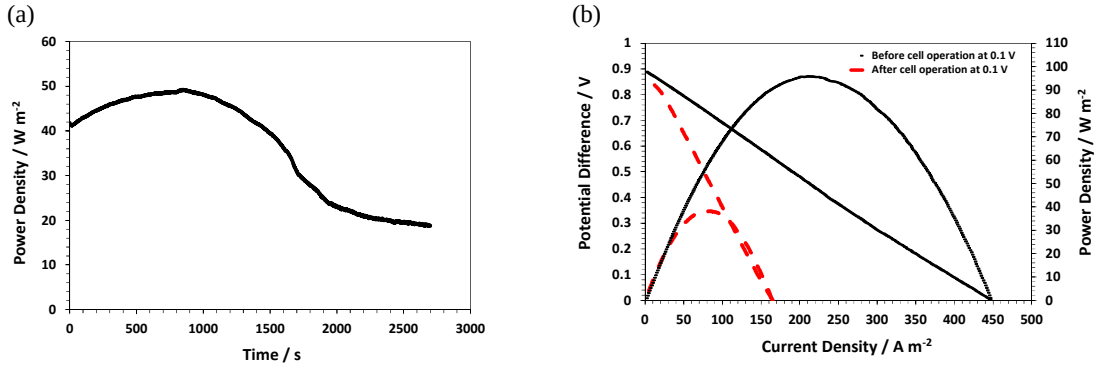

Figure 8: (a) Time dependence of power density of helium stirred SOFC with molten tin anode at 0.1 V and 850 ^{o}C (b) Effect of oxygen dissolution in molten tin on U-j polarization and power density curves of helium stirred SOFC with molten tin anode at 850 ^{o}C

4.4. Effect of Oxygen Accumulation in Molten Tin on Cell Performance

Figure 9a shows the effect of oxygen dissolution on the *U-j* polarization and power density data at 750 °C when 10% oxygen – helium ($10\%O_2 - He$) gas was bubbled through the molten tin, in a separate experiment which was conducted to verify the effect of oxygen accumulation in the molten tin on the current and power densities. In this case the molten tin was first reduced with hydrogen and subsequently flushed with helium to remove the hydrogen, the potential difference was then swept from the open circuit value to zero and back to obtain the initial U-j polarization and power density curves. A $10\%O_2 - He$ gas was afterwards bubbled through the molten tin until it was saturated with oxygen atoms. The potential difference was then swept from the open circuit value to zero and back to obtain the U-j polarization and power density curves again.

As shown in Figure 9a, the oxygen dissolution in molten tin caused a massive decrease in the open circuit potential difference, current and power densities confirming that the observed decrease in open circuit potential difference, current and power densities of Figure 8 were due to the accumulation of dissolved oxygen atoms in the molten tin during the electrochemical dissolution of oxygen in the molten tin anode. Figure 9b shows the effect of oxygen dissolution in molten tin on the impedance spectrum at open circuit; there was no significant change in the ohmic impedance after the molten tin had been saturated with dissolved oxygen atoms, indicating that tin oxide was not deposited on the surface of the YSZ electrolyte.

When helium is replaced with a fuel e.g. methane, the SOFC becomes a methane-fuelled SOFC which can be employed for electricity generation and methane reforming. Hence, further study would consider the direct conversion of methane to electricity and hydrogen in this SOFC with molten tin anode.

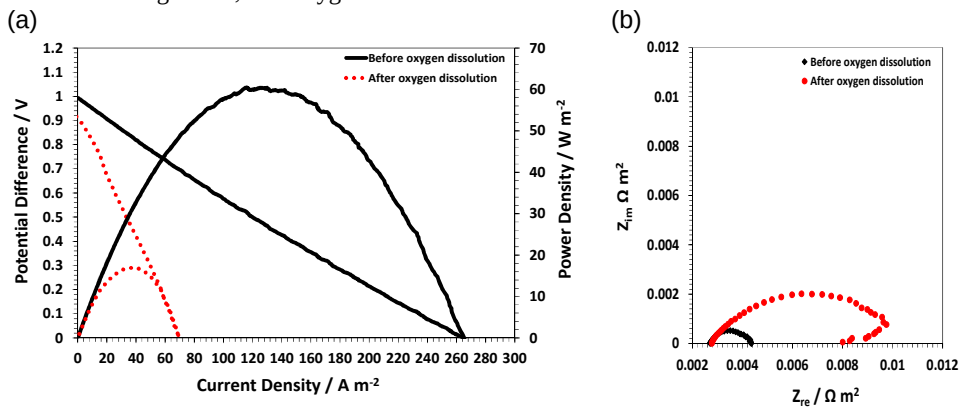

Figure 9: (a) Effect of oxygen dissolution by bubbling $10\%O_2 - He$ through molten tin on U-j polarization and power density curves at 750 ^{o}C (b) Effect of oxygen dissolution by bubbling $10\%O_2 - He$ through molten tin on impedance spectra at open circuit, 750 ^{o}C and frequency range of 10 mHz-10 kHz

5. Conclusions

A $M_{(l)}$-SOFC with a molten metal bath provided a relatively large reservoir of molten metal for oxygen absorption and transport compared to a thin film of molten metal while gas stirring of molten metal enhanced the transport of dissolved oxygen atoms from the YSZ electrolyte | molten metal interface to the bulk molten metal and assisted in preventing oxide formation at the YSZ electrolyte | molten metal interface. A peak power density of ca. 100 W m^{-2} at a potential difference of ca. 0.45 V and current density of ca. 222 A m^{-2} was achieved for a helium-stirred SOFC with molten tin anode. The performance of the cell was controlled by ohmic losses with about 59% of those arising from the inherent difficulty in achieving a low resistance contact at the silver wire (silver wool) current collector | cathode interface. The current and power densities decreased as the oxygen dissolution process progressed due to the resultant accumulation of dissolved oxygen atoms in the molten tin.

Acknowledgements

The authors thank the Petroleum Technology Development Fund, Nigeria for a studentship for Oluseye Agbede at Imperial College London, UK.

References

Abernathy, H., Gemmen, R., Gerdes, K., Koslowske, M. & Tao, T. (2011) Basic properties of a liquid tin anode solid oxide fuel cell, *J. Power Sources.* 196, 4564-4572.

Brett, D.J.L, Atkinson, A., Brandon, N.P., Stephen J. & Skinnerd, S.J. (2008) Intermediate temperature solid oxide fuel cells, *Chem. Soc. Rev.*, 37, 1568–1578.

Cao, T., Wang, H., Shi, Y. & Cai, N. (2014) Direct carbon fuel conversion in a liquid antimony anode solid oxide fuel cell. *Fuel*, 135, 223–227.

Colet Lagrille, M. & Kelsall, G. H. (2013) Thermodynamics and Kinetics of Solid Oxide Fuel Cells with Molten Tin Anodes. *ECS Trans.*, 53 (30)**,** 145-158.

Dantzig, J.A., Clumpner, J.A. & Tyler, D.E. (1980) Degassing of Static Melts by Insoluble Purge Gases. *Metall. Trans. B,* 11 (3), 433-438.

Foger, K., Donelson, R. & Ratnaraj, R. (1999) Demonstration of Anode Supported Cell Technology in kW Class Stack. In: Singhal, S.C. & Dokiya, M. (eds.) *Solid Oxide Fuel Cells (SOFC VI): Proceedings of the Sixth International Symposium*, Electrochemical Society Proceedings, 99-19, Pennington, NJ, Electrochemical Society, pp 95-100.

Gemmen, R., Abernathy, H., Gerdes, K., Koslowske, M., McPhee, W.A. & Tao, T. (2010) Fundamentals of Liquid Tin Anode Solid Oxide Fuel Cell (LTA-SOFC) Operation. In: Bansa, N.P. & Singh, P. (eds.) Advances in Solid Oxide Fuel Cells V, Hoboken, John Wiley & Sons Inc., pp. 37 - 52.

Gorte, R. J., Kim, H. & Vohs, J. M. (2002) Novel SOFC anodes for the direct electrochemical oxidation of hydrocarbon. *J. power sources*, 106**,** 10-15.

Huang, L. Wang, P. Shih, T. & Lios, J. (2002) Effect of degassing treatment on the quality of Al-7Si and A356 Melt. *Mater. Trans*., 43 (11), 2913-2920

Jacob, K.T. (2011) A New Type of SOFC for Conversion of High Temperature Heat to Electricity without Carnot Limitation. *ECS Trans.*, 35 (1), 573-582.

Javadekar, A., Jayakumar, A., Gorte, R.J., Vohs, J.M. & Buttrey, D.J. (2012a) Energy Storage in Electrochemical Cells with Molten Sb Electrodes. *J. Eletrochem. Soc.*, 159 (4), A386-A389.

Javadekar, A., Jayakumar, A., Pujara, R., Vohs, J.M. & Gorte, R.J. (2012b) Molten silver as a direct carbon fuel cell anode. *J. Power Sources* 214, 239-243.

Jayakumar, A., Vohs, J.M. & Gorte, R.J. (2010a) Molten-Metal Electrodes for Solid Oxide Fuel Cells. *Ind. Eng. Chem. Res.*, 49 (21), 10237–10241.

Jayakumar, A., Lee, S., Hornes, A., Vohs, J.M. & Gorte, R.J. (2010b) A Comparison of Molten Sn and Bi for Solid Oxide Fuel Cell Anodes. *J. Electrochem. Soc*., 157 (3), B365-B369.

Jayakumar, A., Küngas, R., Roy, S., Javadekar, A., Buttrey, D.J., Vohs, J.M. & Gorte, R.J. (2011) A direct carbon fuel cell with a molten antimony anode. *Energ. Environ. Sci*. 4, 4133-4137.

Jiang, S.P. (2001) Resistance Measurement in Solid Oxide Fuel Cells. *J. Electrochem. Soc.*, 148 (8), A887-A897

Jiang, S.P., Love J.G. & Apateanu, L. (2003) Effect of contact between electrode and current collector on the performance of solid oxide fuel cells. *Solid State Ionics*, 160 (1), 15-26.

Khurana, S., LaBarbera, M., Fedkin, M.V., Lvov, S.N., Abernathy, H. & Gerdes, K. (2015) Performance evaluation of a liquid tin anode solid oxide fuel cell operating under hydrogen, argon and coal, *J. power sources*, 274, 1049-1054.

Kurokawa, H., Sholklapper, T. Z., Jacobson, C. P., De Jonghe, L. C. & Visco, S. J. (2007) Ceria Nanocoating for Sulfur Tolerant Ni-Based Anodes of Solid Oxide Fuel Cells. *Electrochem. Solid-State Lett.*, 10 (9)**,** B135-B138.

Labarbera, M., Fedkin, M. & Lvov, S. (2011) Liquid Tin-Lead Anode Solid Oxide Fuel Cell Fueled by Coal. *ECS Trans.*, 35 (1)**,** 2725-2734.

Labarbera, M., Khurana, S. Fedkin, M. & Lvov, S., Abernathy, H. & Gerdes, K. (2012) Electrochemical Characterization of Liquid Metal Anode Solid Oxide Fuel Cell. *ECS Transactions*, 41 (12)**,** 103-113.

Matsuzaki, Y. & Yasuda, I. (2000) The poisoning effect of sulfur-containing impurity gas on a SOFC anode: Part I. Dependence on temperature, time, and impurity concentration. *Solid State Ionics*, 132 (3-4)**,** 261-269.

McPhee, W.A.G., Bateman, L., Koslowske, M., Slaney, M., Uzep, Z., Bentley, J., Tao, T. (2011) Direct JP-8 Conversion Using a Liquid Tin Anode Solid Oxide Fuel Cell (LTA-SOFC) for Military Applications. *J. Fuel Cell Sci. Tech.* 8, 041007-1 - 041007-5.

Minh, N. Q. (2004) Solid oxide fuel cell technology—features and applications. *Solid State Ionics*, 174 (1-4)**,** 271-277.

Nikolla, E., Schwank, J. & Linic, S. (2009) Direct Electrochemical Oxidation of Hydrocarbon Fuels on SOFCs: Improved Carbon Tolerance of Ni Alloy Anodes. *J. Electrochem. Soc.*, 156 (11), B1312-B1316.

Offer, G. J., Mermelstein, J., Brightman, E. & Brandon, N. P. (2009) Thermodynamics and Kinetics of the Interaction of Carbon and Sulfur with Solid Oxide fuel Cell Anodes. *J. Am. Ceram. Soc.*, 92**,** 763-780.

Ormerod, R.M. (2003). Solid Oxide Fuel Cells. *Chem. Soc. Rev.*, 32, 17-28.

Papamantellos, D., Lange, K., Okohira, K. & Schenck, H. (1971) A mathematical approach for the mass transfer between liquid steel and an ascending bubble. *Metall. Mater. Trans. B*, 2, 3135-3144.

Sano, M. & Mori, K. (1982) Rate Determining Mechanism of Degassing by Inert Gas Flushing in Molten. *Metal. Trans. JIM*, 23 (8), 440-450

Sarantaridis, D., Chater, R. J. & Atkinson, A. (2008) Changes in physical and mechanical properties of SOFC Ni-YSZ composites caused by redox cycling. *J Electrochem Soc.*, 155 (5), B467-B472.

Sasaki, K., Wurth, J. P., Gschwend, R., Gödickemeier, M. & Gauckler, L. J. (1996) Microstructure-Property Relations of Solid Oxide Fuel Cell Cathodes and Current Collectors: Cathodic Polarization and Ohmic Resistance. *J. Electrochem. Soc.*, 143 (2)**,** 530-543.

Tao, T. (2005) Introduction of Liquid Anode/Solid Oxide Electrolyte Fuel Cell and Its Direct Energy Conversion Using Waste Plastics: Singhal, S.C. & Mizusaki, J. (eds.) *Solid Oxide Fuel Cells IX: The* Electrochemical Society Proceedings, 99-19, Pennington, NJ, Electrochemical Society, pp 353-362.

Tao, T., Bateman, L., Bentley, J. & Slaney, M. (2007) Liquid Tin Anode Solid Oxide Fuel Cell for Direct Carbonaceous Fuel Conversion. *ECS Trans.*, 5 (1), 463-472.

Tao, T., McPhee, W. A., Koslowske, M. T., Bateman, L. S., Slaney, M. J. & Bentley, J. (2008) Advancement in Liquid Tin Anode – Solid Oxide Fuel Cell Technology. *ECS Trans.*, 12 (1), 681-690.

Wang, H., Shi, Y., Yuan, W., Cao, T., Cai, N. & Lang, X. (2013) Performance Characteristics of Liquid Antimony Anode Direct Carbon Fuel Cell. *ECS Trans*., 57 (1), 2913-2922.

Wang, H., Cao, T., Shi, Y., Cai, N. & Yuan, W. (2014a) Liquid antimony anode direct carbon fuel cell fueled with mass-produced de-ash coal, *Energy* 75, 555-559.

Wang, H., Shi, Y. & Cai, N. (2014b) Polarization characteristics of liquid antimony anode with smooth single-crystal solid oxide electrolyte. *J. power sources*, 245, 164-170.

Wang, H., Shi, Y. & Cai, N. (2014c) Characteristics of liquid stannum anode fuel cell operated in battery mode and CO/H_2/carbon fuel mode. *J. power sources*, 246, 204-212.

Warke, V.S., Trggvason, G. & Makhlouf, M.M. (2005) Mathematical modeling and computer simulation of molten metal cleansing by the rotating impeller degasser: Part I. Fluid flow. *J. Mater. Proc. Technol.*, 168, 112-118.